

The supporting information for

Water management by hierarchical structure for highly efficient solar water evaporation

Yukun Sun^a, Xupeng Zong^a, Dan Qu^{a}, Ge Chen^b, Li An^a, Xiayan Wang^a, and Zaicheng Sun^{a*}*

^a Beijing Key Lab for Green Catalysis and Separation, Department of Chemistry and Biology, Beijing University of Technology, Beijing 100124, China

*E-mail: danqu@bjut.edu.cn (Dan Qu)

*E-mail: sunzc@bjut.edu.cn (Zaicheng Sun)

^b Department of Chemical Engineering, Beijing University of Technology, Beijing 100124, China

Content

Table S1. Characterization of various porous materials

Table S2. Estimate relative enthalpy of water in SWE device with different structure

Table S3. Estimate the average water transportation rate in different STOR and RES materials

Table S4. The comparison of SWE performance of this work and the related state-of-the-art studies

Table S5. Results of inferred efficiencies and those calculated from the latent heat of evaporation

Table S6. Words corresponding to the abbreviations in the text

Fig. S1. Comparative images on the mechanism of water evaporation

Fig. S2. The schematic graph for water mass per united area explanation

Fig. S3. IR temperature images of SWE device

Fig. S4. SEM images of Water-restrictive layer (RES) materials

Fig. S5. IR temperature images of SWE device with different RES materials

Fig. S6. X-ray diffraction (XRD) test result

Fig. S7. SEM images of the home-made PTMs

Fig. S8. UV-Vis-NIR absorbance spectrum of home-made PTMs

Fig. S9. Schematic diagram of the device for home-made PTMs intrinsic PCE test

Fig. S10. Intrinsic PCE test results of the home-made PTMs

Fig. S11. Optimization of the thermal management test-1

Fig. S12. Optimization of the thermal management test-2

Fig. S13. Optimization of the thermal management test-3

Fig. S14. Weather condition about the outdoor experiment-1

Fig. S15. Weather condition about the outdoor experiment-2

Fig. S16. Weather condition about the outdoor experiment-3

Fig. S17. Weather condition about the outdoor experiment-4

Fig. S18. Weather condition about the outdoor experiment-5

Fig. S19. Evaluation of water purity using a multimeter with a constant distance between electrodes

Supporting Notes

Note S1. Preparation of photothermal materials used for SWE device

Note S2. ‘One-step filtration processing’ method

Note S3. Water transport measurement

Note S4. Test the intrinsic PCE of home-made PTMs

Note S5 Analysis of energy-balance in steady-state

Note S6. Fabrication of large-scale SWE equipment

Note S7. Outdoor solar steam generation experiment

Note S8. Capillary force about the STOR materials

Table S1. The characterization of various porous materials.

	Q (g g ⁻¹)	S_{pore} (m ² g ⁻¹)	Φ_{pore} (μm)	WMUA (g·m ⁻²)
PU	15.8057	0.1711	328.09	92.38
MF	142.5864	1.7023	191.43	83.76
SS	9.2520	0.2368	36.73	39.07
CC	5.9405	2.8974	1.49	2.05
FP	3.0966	1.9089	1.31	1.62
KP	1.7089	1.6532	0.75	1.03

Q : water content amount, which can be expressed $Q = M_w / M_{\text{dpm}}$, where M_w is the mass of water in the porous materials. $M_w = M_{\text{total}} - M_{\text{dpm}}$. M_{dpm} is the mass of dried porous material, M_{total} is the sum mass of porous material adsorbed water. S_{pore} and Φ_{pore} : surface area and pore diameter of the porous material, which is measured by high-performance full-automatic mercury pressure meter. WMUA: water mass per unit area = Q / S_{pore} (g m⁻²).

Table S2. Estimate relative enthalpy of water in SWE device with different structure.

	Enthalpy (J g ⁻¹)
Bulk water	2256
w/o STOR	2079
w/o PTM layer	1796
w/o PS layer	1796
w/o RES	1921
w/ all layers	1796

The relative enthalpy of water was obtained by this literature.¹

Table S3. Estimate the average water transportation rate in different STOR and RES materials

Material	Transfer rate (kg m ⁻² h ⁻¹)	Material	Transfer rate (kg m ⁻² h ⁻¹)
Suedette sponge	54.82	Kraft paper	1.14
Polyurethane sponge	59.27	Filtrate paper	2.26
Melamine foam	67.54	Cotton cloth	4.36

Table S4. The comparison of SWE performance of this work and the related state-of-the-art studies

Sample	Light intensity (kw m ⁻²)	Water evaporation rate (v _E , kg m ⁻² h ⁻¹)	Conversion Efficiency (η)	Reference
Silicone sponge/MWCNT	1	1.46	92.4%	<i>J. Mater. Chem. A</i> ²
PVA cloth/CNT/EPE foam	1	1.41	88.5%	<i>J. Mater. Chem. A</i> ³
CNF/CNT/E-PS film	1	1.41	95.8%	<i>Nano Energy</i> ⁴
MF/SiO ₂ NPs/cuttlefish juice	1	1.19	85.8%	<i>Nano Energy</i> ⁵
CR-TPE-T	1	1.27	87.2%	<i>Adv. Mater.</i> ⁶
PDA NPs/Air laid paper/Suedette sponge	1	1.84	92.0%	<i>This work</i>
MoS ₂ /EPE foam/Air laid paper	2	1.95	61.0%	<i>J. Mater. Chem. A</i> ⁷
Polypyrrole/Cotton fabric	1	1.20	82.4%	<i>Appl. Therm. Eng.</i> ⁸
Carbon dot/cellulose paper/PS foam	1	2.93	--	<i>J. Mater. Chem. A</i> ⁹
Ti ₂ O ₃ NPs/PVA gel	1	4.0	93.0%	<i>Energy Environ. Sci.</i> ¹⁰

Table S5. Results of inferred efficiencies and those calculated from the latent heat of evaporation

Sample	Evaporation rate (kg m ⁻² h ⁻¹)	Calculated efficiency	Inferred efficiency
PS foam/SS/FP/PDA	1.84	92.0%	89.9%
PS foam/SS/FP/PPy	1.74	87.0%	85.2%
PS foam/SS/FP/GO	1.66	83.0%	81.5%
PS foam/SS/FP/CuS	1.60	79.6%	78.4%
PS foam/MF/FP/GO	1.08	64.1%	62.3%
PS foam/PU/FP/GO	1.09	64.8%	62.6%
PS foam/SS/GO	1.45	72.5%	70.9%
SS/FP/CuS	1.10	57.9%	55.8%
PS foam/SS/FP	0.90	49.6%	46.7%
PS foam/FP/CuS	0.70	38.9%	35.3%

Table S6. Words corresponding to the abbreviations in the text

Number	Abbreviation	Corresponding Word
1	WMUA	Water mass per unit surface area
2	SWE	Solar water evaporation
3	PTM	Photothermal material
4	PCE	Photothermal conversion efficiency
5	RES	Water-restrictive layer
6	STOR	Water storage layer
7	GO	Graphene oxide
8	PPy	Polypyrrole
9	PDA	Polydopamine
10	MF	Melamine foam
11	PU	Polyurethane sponge
12	SS	Suedette sponge
13	CC	Cotton cloth
14	FP	Filter paper
15	KP	Kraft paper

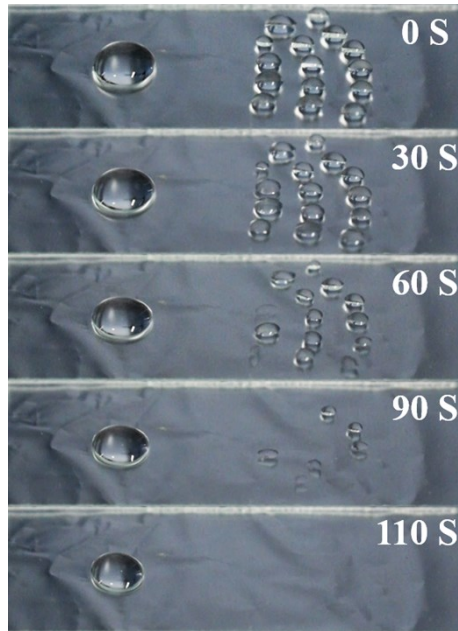


Fig. S1. Comparative images on the mechanism of water evaporation. The digital images revealed the evaporation process of two droplets of the same mass but different volumes.

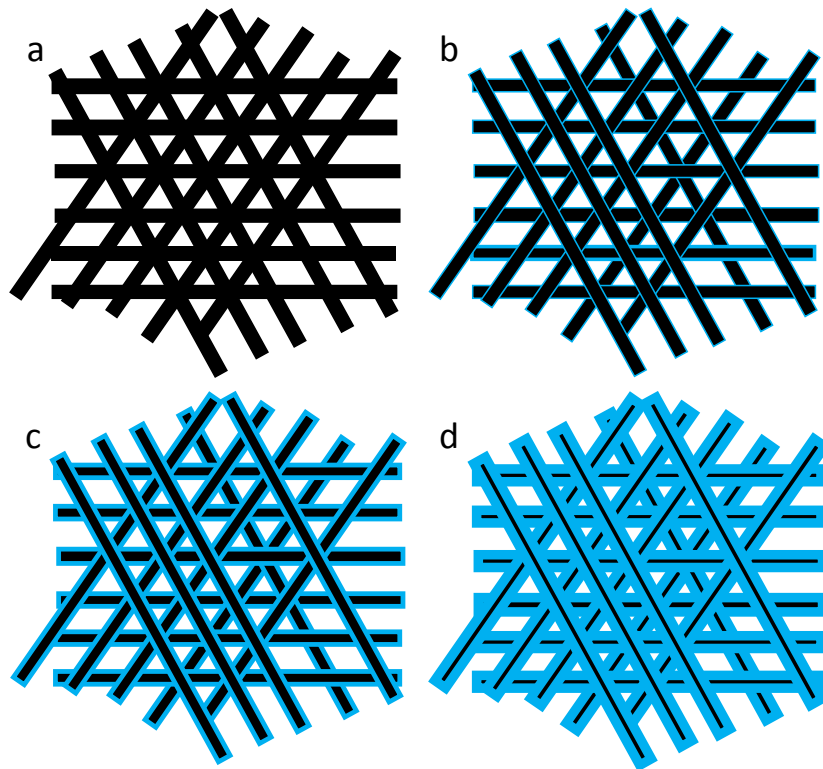


Fig. S2. The schematic graph for water mass per united area explanation. (a) porous structure; (b) porous materials adsorbed a small amount of water, the case of low WMUA; (c) porous material with a moderate amount of water; (d) porous materials with a heavy amount of water, the case of high WMUA. Black stands for the wall of porous structure; blue is the water.

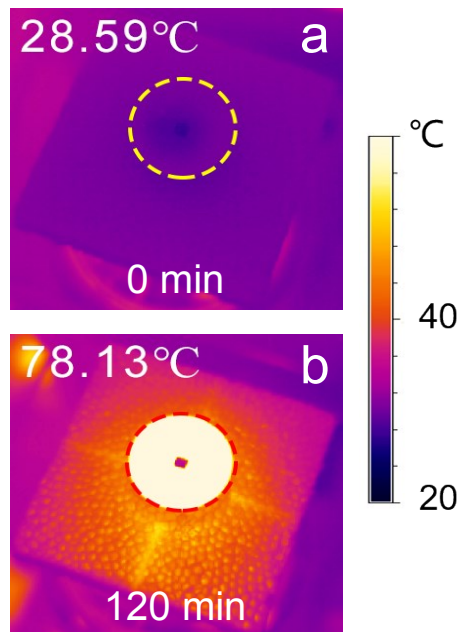


Fig. S3. IR temperature images of SWE device. (a) before and (b) after light irradiation for 120 min without water supply.

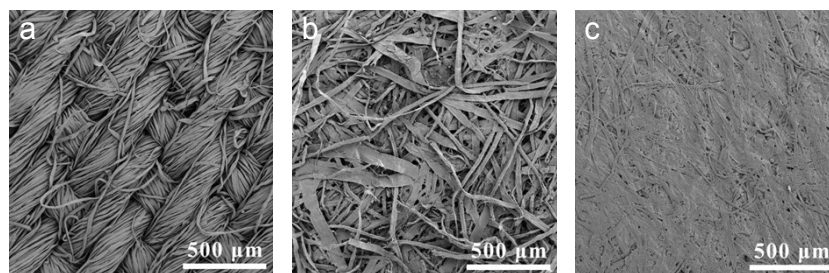


Fig. S4. SEM images of Water-restrictive layer (RES) materials. (a) cotton cloth from top-view (b) filtrate paper from top-view and (c) kraft paper from top-view.

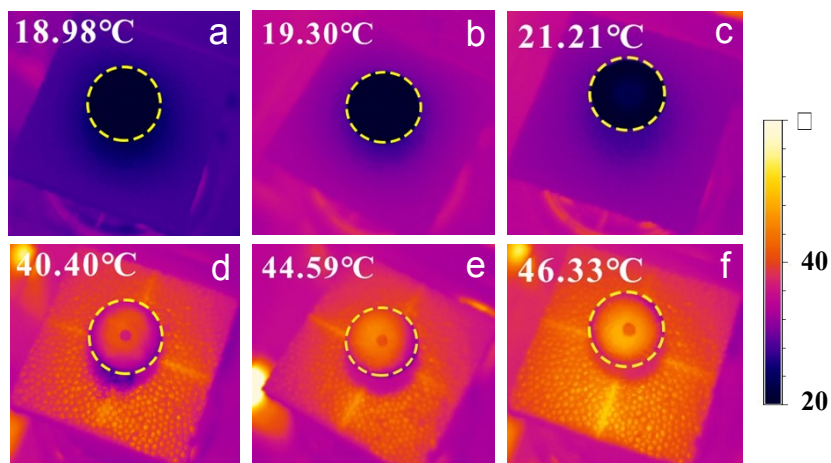


Fig. S5. IR temperature images of SWE device with different RES materials. The images show the SWE device (device structure: suedette sponge / suedette sponge /RES/CuS, RES= cotton cloth, filtrate paper, kraft paper) using (a) cotton cloth and (b) filtrate paper and (c) kraft paper as the RES material respectively when the light is off. IR temperature images of SWE device using (d) cotton cloth and (e) filtrate paper and (f) kraft paper as the water adequate layer material respectively after 2 hours` light irradiation.

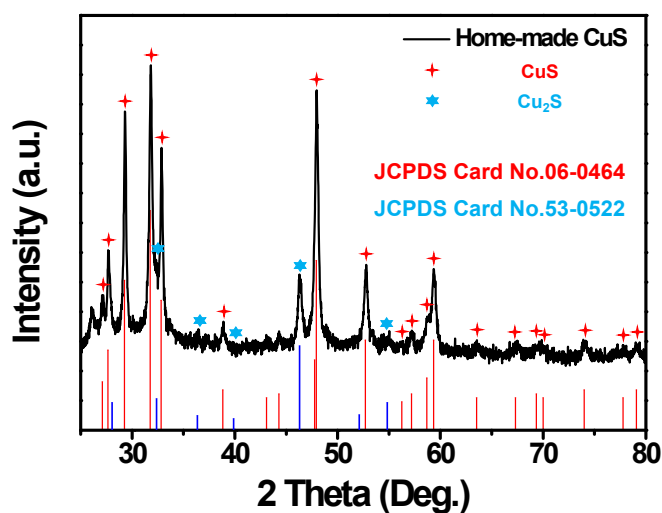


Fig. S6. X-ray diffraction (XRD) test result. The XRD pattern and JCPDS Card NO.06-0464 of the CuS synthesized following the literature.¹¹

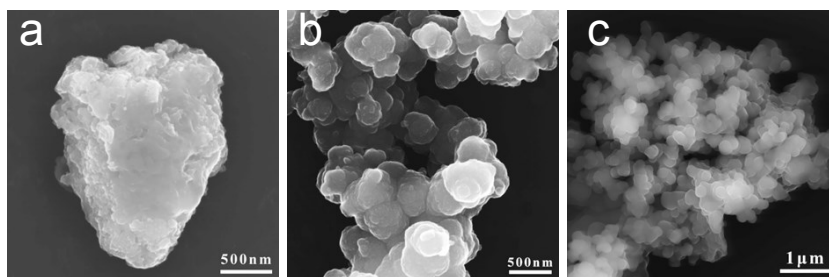


Fig. S7. SEM images of the home-made PTM. (a) CuS, (b) PPy, and (c) PDA.

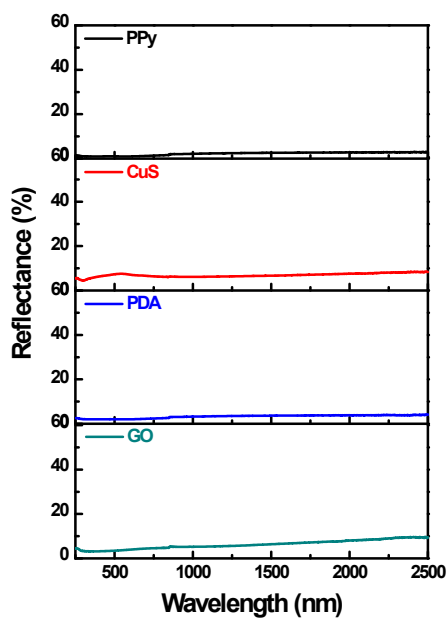


Fig. S8. UV-Vis-NIR absorbance spectrum of home-made PTMs. (a) PPy (b) CuS (c) PDA and (d) GO.

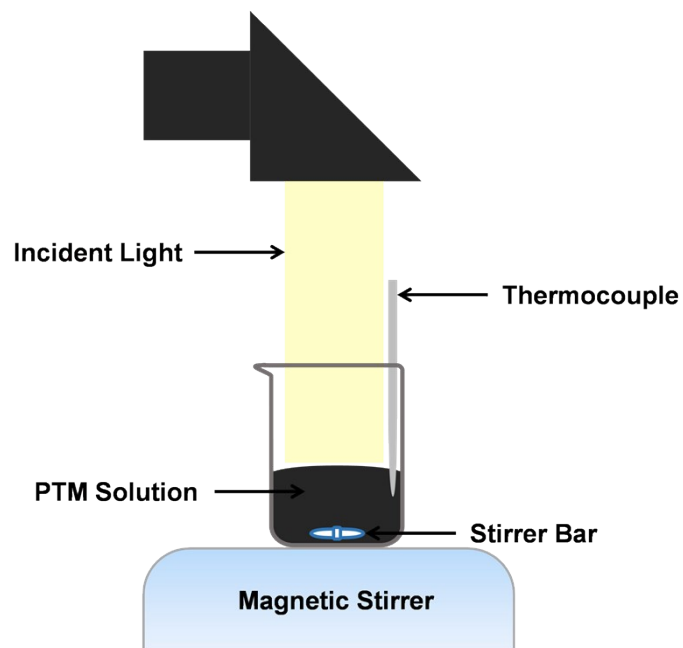


Fig. S9. Schematic diagram of the device for home-made PTMs intrinsic PCE test.

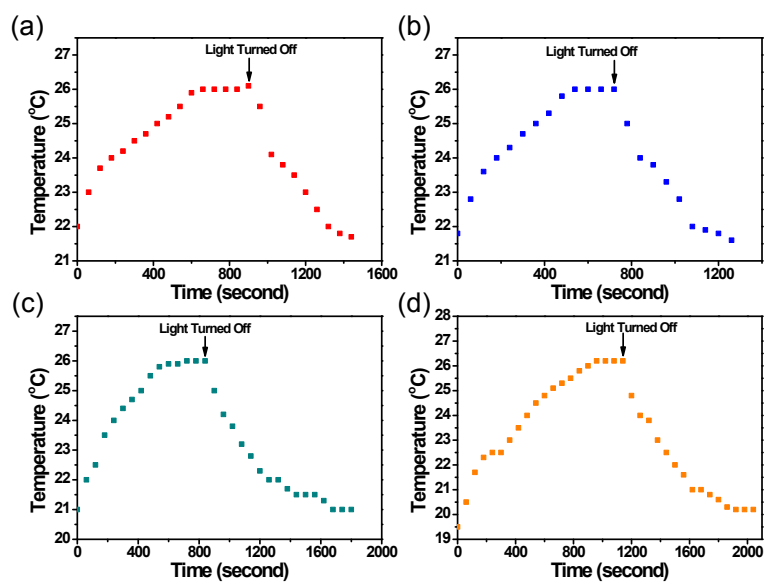


Fig. S10. Intrinsic PCE test results of the home-made PTMs. (a) CuS (b) GO (c) PPy and (d) PDA.

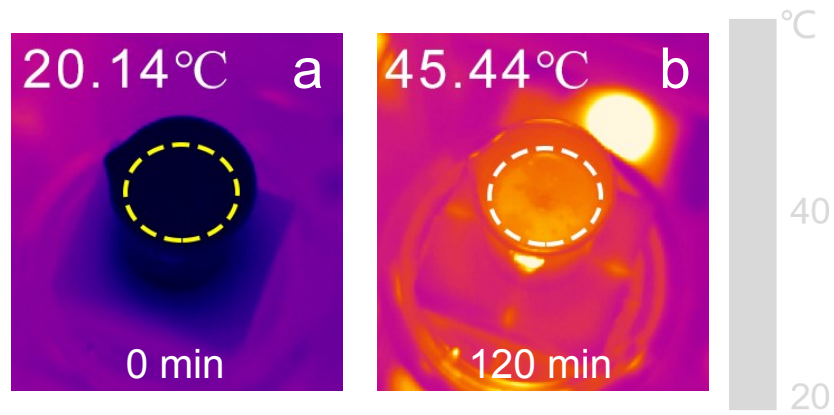


Fig. S11. Optimization of the thermal management test-1. IR temperature images of the SWE device without 1D water transportation channel and PS thermal isolation foam (a) before light irradiation and (b) after 2 hours' irradiation from the top view.

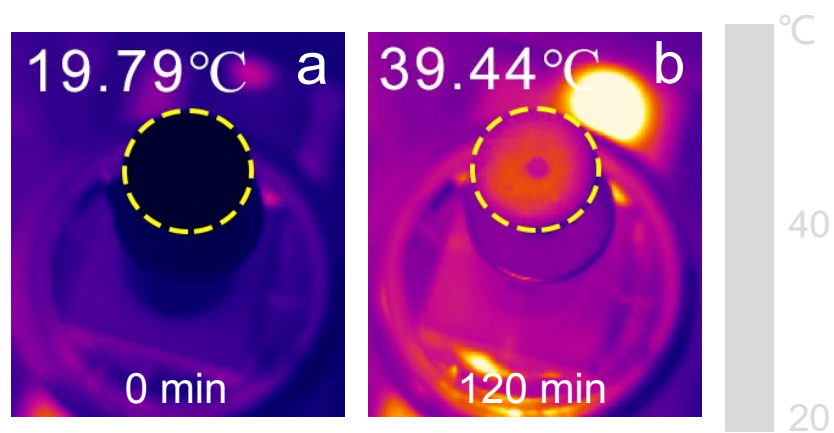


Fig. S12. Optimization of the thermal management test-2. The IR images of the SWE device without PS thermal isolation foam (a) before light irradiation and (b) after 2 hours' irradiation from the top view.

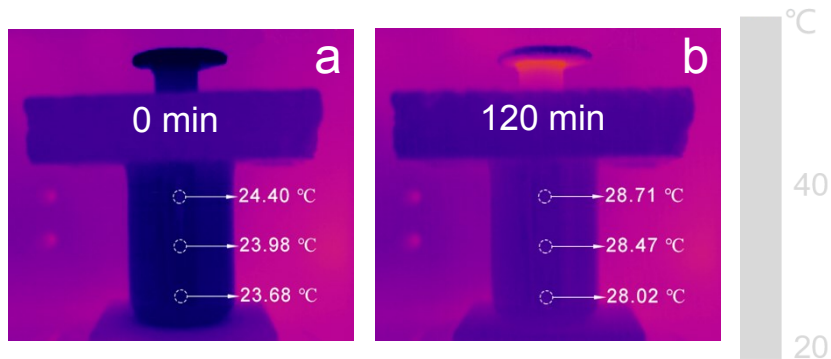


Fig. S13. Optimization of the thermal management test-3. The IR images of the SWE device with whole structure (device structure: PS foam/suedette sponge/STOR/RES/PTM) (a) before light irradiation and (b) after 2 hours' irradiation from the side view.

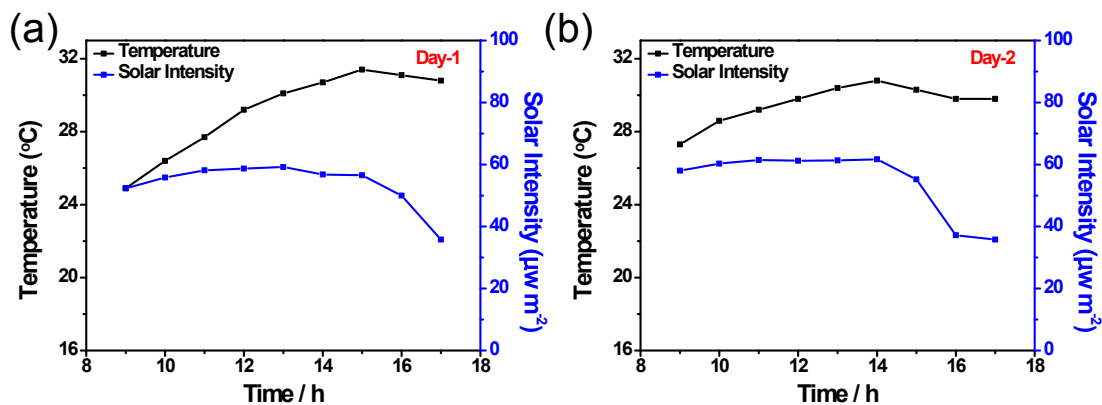


Fig. S14. Weather condition about the outdoor experiment-1. Changes in the ambient temperature (black scatter and line) and solar intensity (blue scatter and line) of the outdoor experiment on (a)Day-1 and (b)Day-2 over time.

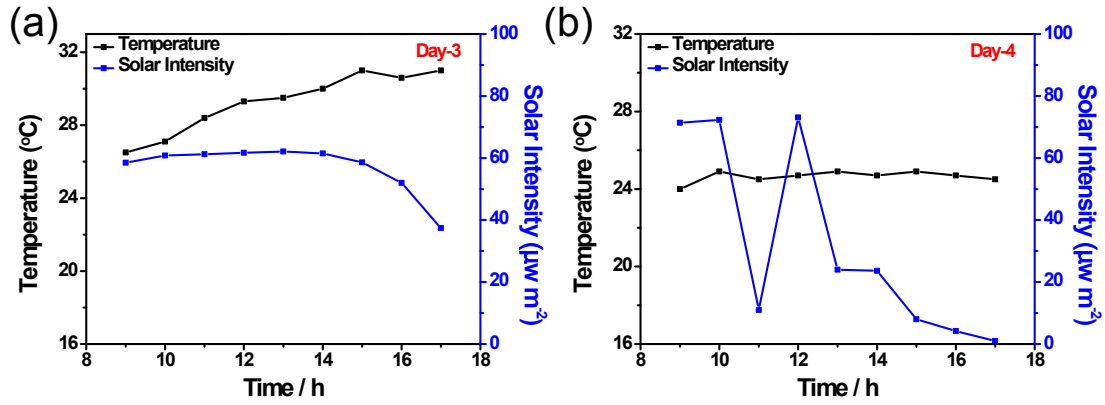


Fig. S15. Weather condition about the outdoor experiment-2. Changes in the ambient temperature (black scatter and line) and solar intensity (blue scatter and line) of the outdoor experiment on (a) Day-3 and (b) Day-4 over time.

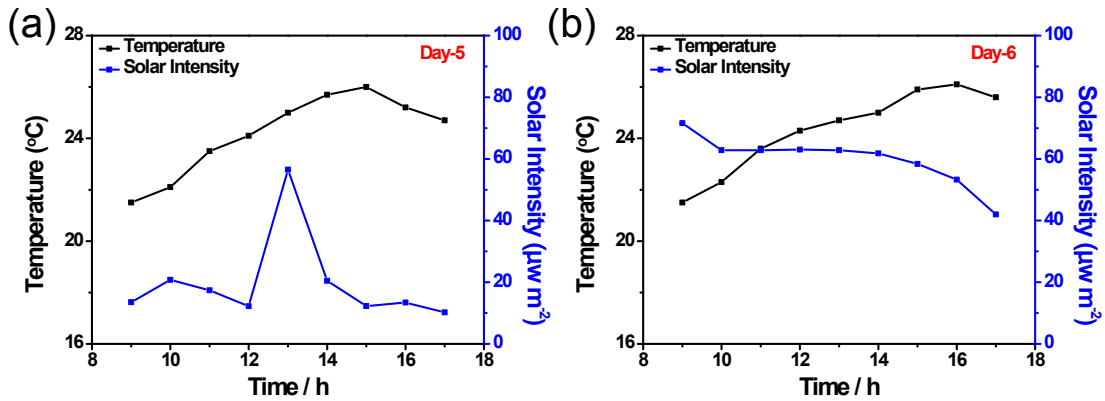


Fig. S16. Weather condition about the outdoor experiment-3. Changes in the ambient temperature (black scatter and line) and solar intensity (blue scatter and line) of the outdoor experiment on (a) Day-5 and (b) Day-6 over time.

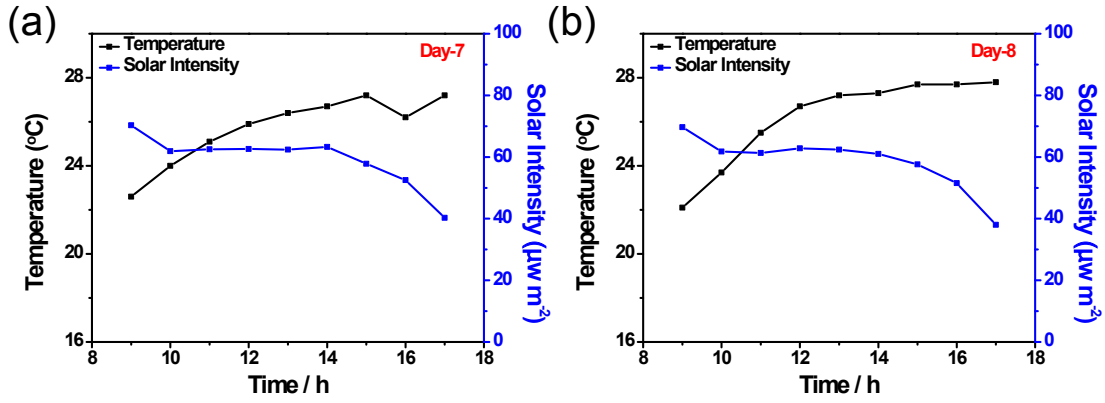


Fig. S17. Weather condition about the outdoor experiment-4. Changes in the ambient temperature (black scatter and line) and solar intensity (blue scatter and line) of the outdoor experiment on (a) Day-7 and (b) Day-8 over time.

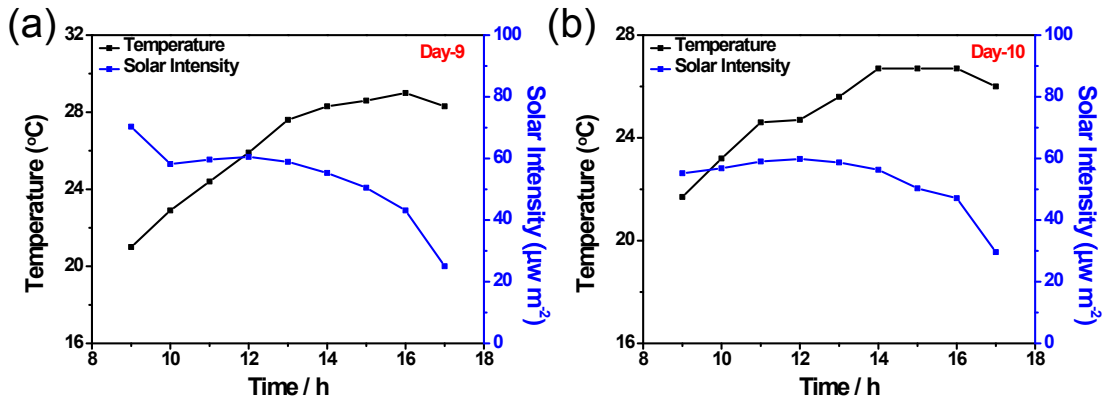


Fig. S18. Weather condition about the outdoor experiment-5. Changes in the ambient temperature (black scatter and line) and solar intensity (blue scatter and line) of the outdoor experiment on (a) Day-9 and (b) Day-10 over time.

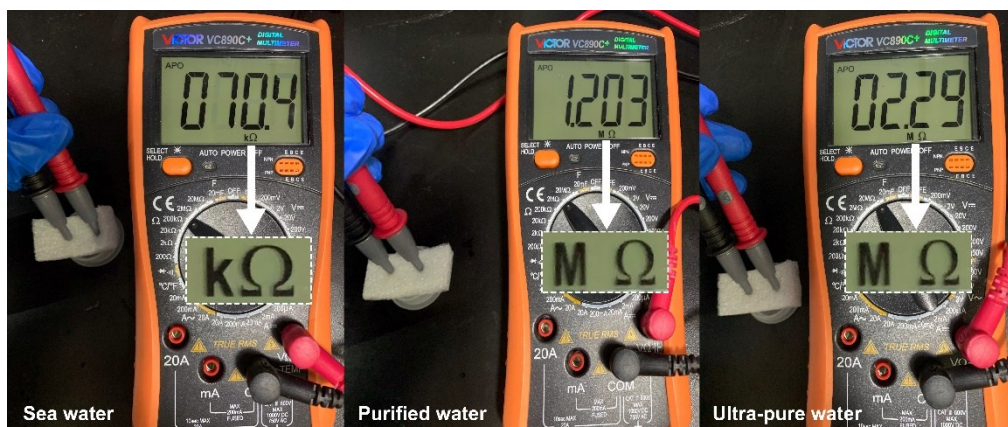


Fig. S19. Evaluation of water purity using resistance meter with a constant distance between electrodes. The electric resistance of Seawater (left panel), purified seawater (middle panel) and the water from Lab ultrapure water system (right panel). The results demonstrated that impurities in seawater can be effectively removed by water evaporation system.

Supporting Notes

Note S1. Preparation of photothermal materials used for SWE device

To achieve the whole SWE device and prove it can be used for common photothermal materials, we selected and fabricated several kinds of photothermal materials. Except that the Graphene oxide (GO) was purchased commercial grade, the other materials were synthesized by the methods in the reference.

Materials

Chemicals including pyrrole, hydrochloric acid (37%), graphene oxide, ferric trichloride, trimethyl-amino methane, dopamine hydrochloride, copper sulfate pentahydrate, sodium hydroxide, glucose, thiourea, polyvinylidene fluoride, and absolute ethanol were purchased from Aladdin Industrial Corporation. The suede sponge, melamine foam, polyurethane sponge, filtrate paper, kraft paper, and cotton were purchased from Alibaba group holding LTD. All chemicals were of analytical grade and used without further purification.

Synthesis of polypyrrole

0.85 mL pyrrole was added into 150 mL of 1M HCl solution and mixed well, then it was placed in an ice water bath, and the FeCl₃/HCl (5 g/50 mL) solution was added dropwise and slowly stirred for 1 h until the solution turned black. Finally, the solution was centrifuged and the supernatant is discarded. The black solid is polypyrrole (PPy).¹²

Synthesis of CuS

Firstly, 1.25 g CuSO₄•5H₂O was dissolved into 50 mL ultra-pure water and stirred evenly at 300 rpm. Then the obtained CuSO₄ solution was heated to 55 °C and kept at this temperature for 2 min. 30 mL NaOH (3 M) solution was poured into the flask rapidly and increase the temperature to 70 °C quickly, the color of solution turned into blue and quickly turn dark blue. After 5 min, 0.3 g glucose was added into the above solution, and made the mixture solution kept 70 °C for 17 min, the Cu₂O has been generated when the color of solution turned red.

Centrifuge the red suspension and retain the precipitate, then wash it with ultra-pure water and absolute ethanol for 3 times to get Cu_2O solid. 0.32 g of the obtained Cu_2O powder was dispersed into 200 mL ultra-pure water (rotation speed was set to 300 rpm), and 0.26 g of thiourea was added, and kept at 90 °C for 4 h, and the CuS was obtained after the reaction was completed.¹¹

Synthesis of Polydopamine

14.7 mL of HCl (0.1 M) was added into 50 mL tris solution (0.1 M) and add ultra-pure water to 100 mL to get the tris-HCl buffer solution (pH = 8.5). 500 mg of dopamine was added into 50 mL of the above solution, the solution turned black after stirring at room temperature (400 rpm) for 24 hours, and the solid remained after centrifugation, and the polydopamine solid powder was obtained by freeze-drying treatment.¹³

Note S2. ‘One-step filtration processing’ method

Firstly, 2 mg PVDF solid was dispersed into 98 mL N-methyl-pyrrolidone (NMP) and ultrasonic until the solid completely dissolved. Then the 2% PVDF solution mixed with 2 mL absolute ethanol and ultrasonic 20 min to mix well. Subsequently, 20 mg photothermal material was taken by electronic balance and dispersed into the mixing solution above, then ultrasonic 20 min to ensure it evenly dispersed. Finally, a piece of filtrate paper ($\square = 34$ mm) was placed in a suction filtrate and then the photothermal material dispersion was filtrated on the filtrate paper.

Note S3. Water transport measurement

In order to achieve the hierarchical water management function of SWE device, water transportation is the first task. So we evaluated the water transport performance in vertical direction and water dispersion performance in horizontal direction of different STOR materials.

Water transport performance test in vertical direction

Firstly, three kinds of STOR materials were chosen and cut into thin strip (100 x 5 x 3 mm), respectively. Then the filtrate paper was cut into a round piece ($\phi = 34$ mm) and was assembled with the thin strip above. Subsequently, the device was placed in the same Rhodamine B (RhB) aqueous solution and ensure that the height of its immersion in the liquid is consistent. After 3 minutes, the height of the liquid raised up in the vertical direction was used to evaluate the water transport properties of different materials. According to the height and area of water transmission in the same time, the average transmission rate of water in different materials can be roughly estimated. The specific results are shown in Table S3.

Water dispersion performance test in horizontal direction

After test the water transport performance in vertical direction we found that the suedette sponge has the best water absorption ability (as shown in Fig. S3c), so we selected the suedette sponge as the water transport channel (make sure enough and same water transportation) to complete the water dispersion performance test in horizontal direction. Three STOR materials were cut into a round piece ($\phi = 34$ mm) respectively and assembled with the water transport channel (suedette sponge). Then the assembled device was placed in same RhB solution and ensure that the height of its immersion in the liquid is consistent. After 3 minutes, record the diffusion of dyes on the surface of three materials and determine which material has the best lateral diffusion capacity for water.

Note S4. Test the intrinsic PCE of home-made Photothermal materials

In order to prove that ordinary photothermal materials (PTMs) are due to the application of the SWE device designed by us, the photothermal conversion efficiency has been greatly improved, we designed a set of experiments to investigate the intrinsic photothermal conversion efficiency of photothermal materials.

The intrinsic PCE of home-made PTMs was measured follows the literature.¹⁴ As the development of SWE device, the solar-thermal conversion efficiency refers more to the entire equipment but not just the PTM. We designed the experiment according to the method reported

in the literature, and investigated the solar-thermal conversion efficiency of PTM dispersed in bulk water.

Theoretical model basis

When the PTM is dispersed in bulk water and irradiated by light, the water temperature will increase significantly compared to irradiating water alone. The change of temperature was mainly attributed to the heat energy converted by the PTM from light irradiation. The heat input from a Xenon lamp (Q_{in}) and dissipation to the external environment (Q_{out}) can be measured and expressed as

$$\sum_i m_i C_i \frac{dT}{dt} = Q_{in} - Q_{out} \quad (1)$$

where m_i and c_i are the mass and specific heat capacity of component i , respectively. T is the temperature, t is time. In the solutions with PTM dispersed, the mass and specific heat capacity of PTM is too less than that of water. Thus equation (1) can be simplified as

$$m_w C_w \frac{dT}{dt} = Q_{in} - Q_{out} \quad (2)$$

where m_w and C_w refer to the mass and specific heat energy of water, respectively. And the rate of heat produced by PTM upon Xenon lamp irradiation can be expressed as

$$Q_{in} = (I_0 - I_{tr})\eta \quad (3)$$

where I_0 is the incident light power (measured by a radiometer), I_{tr} is the power of light which is transmitted through the solution, and η is the light-to-heat conversion efficiency.

The heat energy dissipated to the ambient can be calculated by

$$Q_{out} = \sum hS[T(t) - T_0] \quad (4)$$

where h is the heat transfer efficiency, S is the interface surface area between the PTM and external ambient, $T(t)$ is the temperature at time t , and T_0 refers the environmental temperature. Determine $\Delta T \equiv T(t) - T_0$, equation (2) can be simplified as

$$\frac{d \Delta T}{dt} = \frac{(I_0 - I_{tr})\eta}{m_w C_w} - \frac{\sum hS}{m_w C_w} \Delta T \quad (5)$$

From here, we define $B = \sum hS / m_w C_w$ as the fixed heat dissipation rate from PTM solution to the external environment, which can be obtained by measuring the decreasing temperature profile after turn off the Xenon lamp. The temperature trace in this regime can be found by setting $(I_0 - I_{tr}) = 0$ in equation (5) and solving for $T(t)$ using the limit $T(0) = T_m$. The result is

$$T(t) = T_0 + (T_m - T_0) \exp(-Bt) \quad (6)$$

where T_m is the highest temperature the solution can reach when the Xenon lamp is off.

It's easy to understand that when Q_{in} is equal to Q_{out} , the solution temperature will remain constant. Therefore, a new equation can be obtained by setting equation (5) = 0

$$\frac{(I_0 - I_{tr})\eta}{m_w C_w B} = \Delta T \quad (7)$$

Thus if the mass of solution does not change for each measurement, and B was obtained from equation (6), then η can be determined by plotting the temperature increase as a function of decreasing incident light power.

Intrinsic photothermal conversion

5 mg of PTM was dissolved in 15 mL deionized water (DIW), as shown in Fig. S8, a thermocouple was inserted into the beaker containing 15 mL PTM solution to obtain temperature changes over time. And the solution was kept stirring to ensure the temperature distribution uniform upon Xenon lamp irradiation. A Xenon lamp with an AM1.5G filtrate (PLS-SXE 300, Beijing Trusttech Co. Ltd, China) was used to illuminate the PTM solution. A control experiment with pure water loaded in the beaker was taken to ensure the incident light does not cause an obvious temperature increase in the water. Therefore, the temperature change was definitely caused by the heat converted from PTM upon light irradiation.

Note S5. Analysis of energy-balance in steady-state

The total input energy is mainly dissipated in five forms, except for the latent heat of water evaporation, the calculation methods for the remaining four energy dissipation are as follows.

(1) *Sensible heat:*

$$Q_{sen} = C\dot{m}\Delta T \quad (8)$$

where Q_{sen} is the sensible heat of water evaporation ($\text{kJ m}^{-2} \text{h}^{-1}$), C is the specific heat capacity of water ($\sim 4.2 \text{ kJ kg}^{-1} \text{K}^{-1}$), \dot{m} is the evaporation rate of PTM ($\text{kg m}^{-2} \text{h}^{-1}$), and ΔT is the temperature difference between the PTM surface and the bulk water.

(2) *Reflection energy loss:*

Part of the incident light can be absorbed by the PTM on the top layer of SWE device, and the remaining light was reflected and transmitted by the PTM. Since the device is thick enough, the light that can pass through can be ignored. Therefore, except for the reflected light, the rest of the light can be absorbed by the PTM and converted into heat energy. And the reflection energy loss was obtained from the UV-Vis-NIR spectrometer.

(3) *Conductive heat loss:*

It should be noted that the conductive heat loss can be ignored not only due to the 1D water transport channel material was always immersed in the bulk water and keep the temperature consist with it, but also the size of 1D water transport channel is smaller (2 mm x 2 mm x 20 mm) than the whole evaporator.

(4) *Radiation heat loss:*

The radiation heat loss can be calculated by Stefan-Boltzmann law.

$$Q_{rad} = 3600 * 0.46 * \varepsilon\sigma(T_{max} - T_0) \quad (9)$$

where Q_{rad} denotes radiation heat loss, ε is the emissive rate of PTM (~ 0.85), σ is the Stefan-Boltzmann constant ($5.67 \times 10^{-8} \text{ W m}^{-2} \text{K}^{-4}$), T_{max} and T_0 is the temperature of PTM surface and surroundings, respectively. It should be noted that a factor of 0.46 was used due to the irradiation area during the evaporation process accounts for 0.46 of the total sample area.

(5) *Convection heat loss:*

The convection heat loss can be calculated by the following equation:

$$Q_{conv} = 3600 * 0.46 * h(T_{max} - T_0) \quad (10)$$

where h is the natural convective heat transfer coefficient ($\sim 5 \text{ W m}^{-2} \text{ K}^{-1}$), and T_{max} and T_0 is the temperature of PTM surface and surroundings, respectively.

According to the above calculation method, the overall PCE can be obtained by the following equation:

$$\eta_{overall} = 100\% - R\% - \frac{Q_{sen} + Q_{rad} + Q_{conv}}{3600I_0} \quad (11)$$

The energy conversion efficiency calculated based on the latent heat of evaporation is compared with the result obtained by inferred, and they show similar results (Table S5), which demonstrate the efficiency calculation method of this work is reliable.

Note S6. Fabrication of large-scale SWE equipment

Step 1 Firstly, 75 mL 2% PVDF solution was prepared, then it was mixed with 78.5 mL ethanol and ultrasonic the solution for 25 min. Subsequently, 390 mg PDA powder was poured into the solution above and ultrasonic for 30 min. Next a piece of filtrate paper ($\square = 120 \text{ mm}$) was placed in a suction filtrate and then the PDA dispersion was filtrated on the filtrate paper. Finally, the filtrate paper loaded with photothermal material was placed into the oven ($\sim 60^\circ\text{C}$) to dry overnight.

Step 2 Firstly, cut a piece of suedette sponge with a diameter of 150 mm and then stitch it together with the dried filtrate paper. Dig 4 holes ($11 \times 8 \text{ mm}$) at equal distances on the assembled filtrate paper and suedette sponge. Then cut another suedette sponge into 4 strips of the same size ($60 \times 11.5 \times 8.5 \text{ mm}$), and install it into the treated filtrate paper on.

Step 3 Cut a piece of PS foam into a size of $150 \times 150 \times 20 \text{ mm}$, and dig four holes on it. The positions of the holes correspond to the holes on the filtrate paper. Then, as shown in Fig. S6 (b), the materials produced in step 2 and 3 are assembled into large-scale SWE equipment.

Note S7. Outdoor solar steam generation experiment

The large-scale SWE equipment can achieve a good solar steam generation property in outdoor environments. In Chaoyang district, Beijing, China, the outdoor experiment was conducted in September 2020. The average ambient temperature was about 29.1°C on day-1 (Fig. S13a) (temperature data of the outdoor experiment came from the official website of the National Meteorological Center), we used the large-scale SWE equipment collected a total of 57.12 g water in 8 h. In order to ensure the reliability of data, we repeated this experiment 10 times, and the ambient temperature and solar intensity of everyday was recorded (Fig. S14-S17).

Note S8. Capillary force about the water-storage layer materials

The relationship of the height of water with the radius of tube:

The height h of a liquid column is given by Jurin's law:

$$h = \frac{2\gamma\cos\theta}{\rho gr} \quad (12)$$

where γ is the liquid-air surface tension (force/unit length), θ is the contact angle, ρ is the density of liquid (mass/volume), g is the local acceleration due to gravity (length/square of time), and r is the radius of tube. Thus, the thinner the space in which the water can travel, the further up it goes.

For a water-filled glass tube in air at standard laboratory conditions, $\gamma = 0.0728$ N/m at 20 °C, $\rho = 1000$ kg/m³, and $g = 9.81$ m/s². For these values, the height of the water column is

$$h \approx \frac{1.48 \times 10^{-5} m^2}{r} \quad (13)$$

Thus for a 2 m radius glass tube in lab conditions given above, the water would rise an unnoticeable 0.007 mm. However, for a 2 cm radius tube, the water would rise 0.7 mm, and for a 0.2 mm radius tube, the water would rise 70 mm.

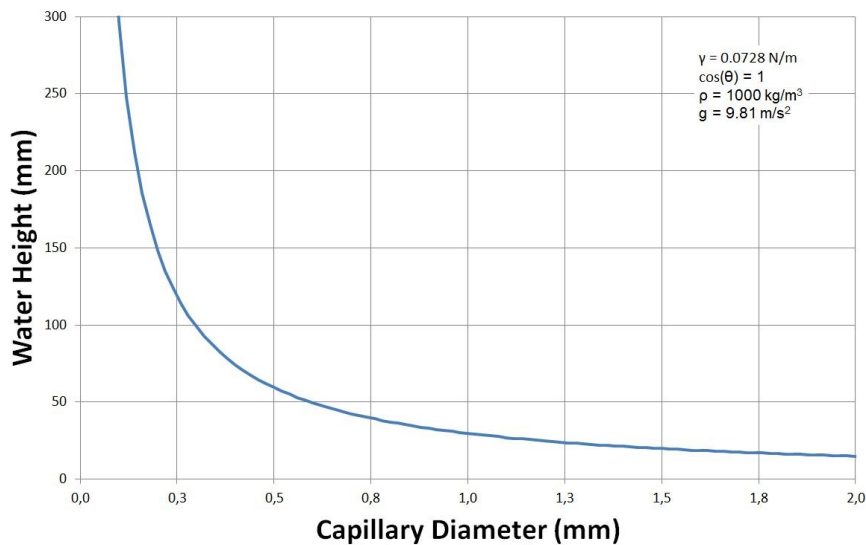
If we treat the materials as glass tube besides pore size difference

For melamine foam with average 325 μ m pore size, water can rise ~92 mm.

For polyurethane sponge with 200 μm pore size, water can rise ~ 148 mm

For suedette sponge with 50 mm pore size, water can rise ~ 592 mm, for the suedette sponge has mesoporous in the wall which will enhance the water transport further.

Considering the contact angle, suedette sponge is a kind of hydrophilic materials polyvinyl alcohol.



Analyzing the SWE system, it includes three procedures: (1) photo thermal material (PTM) absorbs the light and converts into thermal heat (PTM); (2) heat transfer from PTM to water; and (3) water evaporation. It requires the PTM adsorb the light which cover the whole solar spectrum and low transmittance and reflectance. Besides that, the photothermal conversion efficiency is another critical factor for the PTM. At the same time, it is expected to avoid of other kinds of energy loss such as emission. Secondly, it demands the close contact between water and PTM to achieve highly efficient heat transfer. The large surface area and hydrophilic interface are highly preferring. Heat loss through radiation, convection and conduction is expected to be avoided. Low emissivity reduce the thermal radiation and low conduction is beneficial to the localized high temperature. Thirdly, the heat received by water mainly used for evaporation and temperature increasing. Increasing the interface between water and air will beneficial to the evaporation. Based on the above analysis, the PTM and hierarchical

nanostructure to achieve the water management play a decisive role for the solar water evaporation.

References

1. F. Zhao, X. Zhou, Y. Shi, X. Qian, M. Alexander, X. Zhao, S. Mendez, R. Yang, L. Qu and G. Yu, *Nature Nanotechnology*, 2018, **13**, 489-495.
2. T. Hu, L. Li, Y. Yang and J. Zhang, *Journal of Materials Chemistry A*, 2020, **8**, 14736-14745.
3. Y. Xia, Y. Li, S. Yuan, Y. Kang, M. Jian, Q. Hou, L. Gao, H. Wang and X. Zhang, *Journal of Materials Chemistry A*, 2020, **8**, 16212-16217.
4. K. Li, M. Gao, Z. Li, H. Yang, L. Jing, X. Tian, Y. Li, S. Li, H. Li, Q. Wang, J. S. Ho, G. W. Ho and P.-Y. Chen, *Nano Energy*, 2020, **74**, 104875.
5. Z. Li, J. Zhang, S. Zang, C. Yang, Y. Liu, F. Jing, H. Jing, J. Hu, C. Wang and Y. Zhou, *Nano Energy*, 2020, **73**, 104834.
6. G. Chen, J. Sun, Q. Peng, Q. Sun, G. Wang, Y. Cai, X. Gu, Z. Shuai and B. Z. Tang, *Advanced Materials*, 2020, **32**, 1908537.
7. R. Chen, X. Wang, Q. Gan, T. Zhang, K. Zhu and M. Ye, *Journal of Materials Chemistry A*, 2019, **7**, 11177-11185.
8. D. Hao, Y. Yang, B. Xu and Z. Cai, *Appl Therm Eng*, 2018, **141**, 406-412.
9. Z. Wang, W. Tu, Y. Zhao, H. Wang, H. Huang, Y. Liu, M. Shao, B. Yao and Z. Kang, *Journal of Materials Chemistry A*, 2020, **8**, 14566-14573.
10. Y. Guo, X. Zhao, F. Zhao, Z. Jiao, X. Zhou and G. Yu, *Energy & Environmental Science*, 2020, **13**, 2087-2095.
11. X. Wu, M. E. Robson, J. L. Phelps, J. S. Tan, B. Shao, G. Owens and H. Xu, *Nano Energy*, 2019, **56**, 708-715.
12. D. D. Hao, Y. D. Yang, B. Xu and Z. S. Cai, *Appl Therm Eng*, 2018, **141**, 406-412.
13. H. Lee, S. M. Dellatore, W. M. Miller and P. B. Messersmith, *Science*, 2007, **318**, 426.
14. K. Jiang, D. A. Smith and A. Pinchuk, *The Journal of Physical Chemistry C*, 2013, **117**, 27073-27080.